phys. stat. sol. (b) **175**, 433 (1993)

Subject classification: 72.10 and 73.40; 72.20; S7.12; S7.15

Shanghai Institute of Metallurgy, Chinese Academy of Sciences, Shanghai[1])

Subband Effects on High-Field Electron Transport in Quasi-One-Dimensional Systems

By

X. F. WANG and X. L. LEI

A detailed calculation of electron transport in $Al_xGa_{1-x}As/GaAs$ quantum wires by the use of a balance-equation approach, considering all possible acoustic and optical phonon scattering and taking fifteen subbands into account, is reported. Crossover from one dimension (1D) to three dimensions (3D) in both low- and high-field regimes is studied by investigating mobility and electron temperature as functions of the radius of quantum wire. At low temperatures, the linear mobility of a quasi-1D electron system may be ten times higher or ten times lower than that of a 3D system depending on the relative position of the Fermi energy to subbands. At very high electric field, the difference in the transport behavior of quantum wires with differing radii and that of a 3D system disappears as a result of high electron temperature and drift velocity.

1. Introduction

With remarkable developments in semiconductor technology, it has become possible to confine electrons in extremely small semiconductor quantum wires with lateral extension comparable to the electron de Broglie wavelength (≈ 10 nm) [1 to 3]. In addition to extensively studied Ohmic conductance of electrons [5 to 10], high-field transport in a quantum wire was explored by the Monte Carlo method [11]. Recently, multisubband effects in a quantum wire have attracted much attention both theoretically [7, 11, 12 to 16] and experimentally [3]. Most of the previous investigations, however, were focused on longitudinal optical (LO) phonons, which play an important role at high temperature ($T_e > 40$ K). Besides, the existing studies about subband effects on transport are mainly limited to the electron–impurity system [12] or limited to low-field conduction [12 to 16]. The more interesting case of high-field transport with dominant electron–phonon coupling has not yet been reported in the literature.

The purpose of this paper is to discuss the subband effects on the electron transport in quantum wires and to analyze the crossover from 1D to 3D behavior in both low and high fields. For the sake of simplicity, cylindrical GaAs wires surrounded by AlGaAs are considered where the transverse dimension can be described by one parameter, the radius of the wire. We first formulate the resistivity of electrons in quantum wires considering both inter- and intrasubband impurity and phonon scatterings taking advantage of the balance-equation method of Lei and Ting [17], and then calculate the transport properties in quantum wires, taking account of fifteen subbands.

To facilitate comparison between the transport in quantum wires and that in bulk materials, we focus on the influence of phonon scatterings. When the electron wire density

[1]) 865 Changning Road, Shanghai 200050, People's Republic of China.

is not too high, the subband effect and the crossover are observed mainly in quantum wires with radius larger than 5 nm. In these systems, the surface phonons and the confined phonons can be neglected [7]. In this paper we assume that electrons interact only with bulk phonons, which includes longitudinal acoustic (LA) phonons (through deformation potential and piezoelectric interaction), transverse acoustic (TA) phonons (through piezoelectric interaction), and longitudinal optical (LO) phonons (through deformation potential and Fröhlich interaction).

2. Balance Equations in Quantum Wires

As a simple model, we consider electrons confined in a cylindrical quantum wire of radius ϱ and length L_z. The electron energy in the quantum wire can be expressed as

$$\varepsilon_n(k_z) = \varepsilon_n + \frac{k_z^2}{2m^*}, \tag{1}$$

where k_z is the one-dimensional wave vector, ε_n the confined 2D n-th subband energy, and m^* the electron mass. The wave function of the transverse subband state is given by

$$\varphi_n = \psi_l^m(\boldsymbol{r}_\parallel) = C_l^m \, \mathrm{J}_m\left(\frac{x_l^m}{\varrho}\, \boldsymbol{r}_\parallel\right) \mathrm{e}^{im\varphi}; \qquad \begin{cases} m = \ldots, -3, -2, -1, 0, 1, 2, 3, \ldots \\ l = 1, 2, 3, \end{cases} \tag{2}$$

where $C_l^m = (\sqrt{\pi}\varrho y_l^m)^{-1}$ is the normalization factor, $\boldsymbol{r}_\parallel$ denotes the transverse coordinate, x_l^m represents the l-th zero of the m-th-order Bessel function, i.e. $\mathrm{J}_m(x_l^m) = 0$, and $y_l^m = \mathrm{J}_{m+1}(x_l^m)$. The corresponding eigenenergy is $\varepsilon_n \equiv \varepsilon_l^m = (x_l^m)^2/(2m^*\varrho^2)$. In the following paragraphs, we use the subscript n to denote $\{{}^m_l\}$.

When a uniform electric field $\boldsymbol{E}$ is applied along the wire, the electrons will drift along the z-direction. Introducing the center-of-mass momentum and coordinate variables P, Z in z-direction, we can express the Hamiltonian in the form

$$H = H_\mathrm{c} + H_\mathrm{e} + H_\mathrm{ph} + H_\mathrm{ep} + H_\mathrm{ei}, \tag{3}$$

where

$$H_\mathrm{c} = \frac{P^2}{2M} - N_1 EZ \tag{4}$$

and

$$H_\mathrm{e} = \sum_{n,k_z,\sigma} \varepsilon_n(k_z)\, C^\dagger_{nk_z\sigma} C_{nk_z\sigma} + \sum_{nn'm'm} \sum_{k_z k_z', q_z} \sum_{\sigma\sigma'} U_{n,n',m',m}(q_z)\, C^\dagger_{n,k_z+q_z,\sigma} C^\dagger_{n',k_z'-q_z,\sigma'} C_{m',k_z',\sigma'} C_{m,k_z,\sigma} \tag{5}$$

are the center-of-mass and relative electron Hamiltonian, respectively, $M = N_1 m^*$, N_1 is the electron wire density,

$$U_{n,n',m',m}(q_z) = \frac{e^2}{4\pi\epsilon_0 \varkappa L_z} \int \mathrm{d}\boldsymbol{r}_\parallel \, \mathrm{d}\boldsymbol{r}'_\parallel \, \varphi_n^*(\boldsymbol{r}_\parallel)\, \varphi_{n'}^*(\boldsymbol{r}'_\parallel)\, \varphi_{m'}(\boldsymbol{r}'_\parallel)\, \varphi_m(\boldsymbol{r}_\parallel)\, \mathrm{K}_0(|q_z|\, |\boldsymbol{r}_\parallel - \boldsymbol{r}'_\parallel|)$$

is the Coulomb interaction, and $\varkappa$ is the low-frequency dielectric constant of the quantum wire material, K_0 is the modified Bessel function of zeroth order.

$$H_{\mathrm{ph}} = \sum_{q,\lambda} \Omega_{q,\lambda} b^{\dagger}_{q\lambda} b_{q\lambda} \tag{6}$$

is the phonon Hamiltonian, $\Omega_{q,\lambda}$ the phonon energy, and $b^{\dagger}_{q\lambda}(b_{q\lambda})$ are creation (annihilation) operators of phonon with wave vector q in branch λ; $q \equiv (q_{\|}, q_z)$, $q_{\|} \equiv (q_x, q_y)$.

In (3)

$$H_{\mathrm{ei}} = \sum_{n,n'} \sum_{k_z,q_z,a} \bar{U}(n, n', q_z)\, C^{\dagger}_{n,k_z} C_{n',k_z-q_z}\, \mathrm{e}^{-iq_z Z_a} \tag{7}$$

represents the impurity–electron interaction where $\bar{U}(n, n', q_z)$ is the impurity potential and Z_a the z-coordinate of the impurity. Considering an impurity located at $R_{\|}$ away from the center of the quantum wire with charge $Z_e|e|$, we have

$$\bar{U}(n, n', q_z) = \frac{Z_e e^2}{2\pi\epsilon_0 \varkappa L_z} \int \mathrm{d}r_{\|} \varphi^*_n(r_{\|})\, \varphi_{n'}(r_{\|})\, \mathrm{K}_0(|R_{\|} - r_{\|}|\,|q_z|)\,.$$

In (3)

$$H_{\mathrm{ep}} = \sum_{n,n'} \sum_{q,\lambda} M(n, n', q, \lambda)\, (b_{q\lambda} + b^{\dagger}_{-q\lambda})\, C^{\dagger}_{n,k_z+q_z} C_{n',k_z} \tag{8}$$

stands for the coupling between electrons and bulk phonons, and

$$M(n, n', q, \lambda) = M(q, \lambda)\, F_{n,n'}(q_{\|}) \tag{9}$$

is the corresponding coupling matrix element with

$$F_{nn'}(q_{\|}) \equiv F^{mm'}_{ll'}(q_{\|}) = 2 \int_0^1 \xi\, \mathrm{d}\xi\, \frac{1}{y^m_l y^{m'}_{l'}}\, \mathrm{J}_m(x^m_l \xi)\, \mathrm{J}_{m'}(x^{m'}_{l'} \xi)\, \mathrm{J}_{|m-m'|}(q_{\|} \varrho \xi)\,.$$

$M(q, \lambda)$ is the electron–phonon coupling matrix element in 3D Fourier representation and $F_{nn'}$ is the form factor of the quasi-1D electron system.

Following the treatment of the Lei-Ting balance equation theory, we use two parameters, v_{d}, the drift velocity, and T_{e}, the electron temperature, to describe the transport system under the influence of an electric field E. The force- and energy-balance equations in steady state are given by

$$N_1 eE + F(v_{\mathrm{d}}) = 0\,, \tag{10}$$

$$v_{\mathrm{d}} F(v_{\mathrm{d}}) + W(v_{\mathrm{d}}) = 0\,. \tag{11}$$

Here the frictional force $F(v_{\mathrm{d}})$ due to impurity and phonon scatterings can be expressed as

$$F(v_{\mathrm{d}}) = n_i \sum_{n,n',q_z} |U(n, n', q_z)|^2\, q_z \Pi_2(n', n, q_z, \omega_0) + 2 \sum_{n,n',q_z,\lambda} |M(n, n', q, \lambda)|^2\, q_z \Pi_2(n', n, q_z, \Omega_{q,\lambda} + \omega_0) \left[n\left(\frac{\Omega_{q,\lambda}}{T}\right) - n\left(\frac{\Omega_{q,\lambda} + \omega_0}{T_{\mathrm{e}}}\right) \right] \tag{12}$$

assuming the impurities to be randomly distributed along the quantum wire with wire density n_i. The energy dissipation rate $W(v_d)$ is given by

$$W(v_d) = 2 \sum_{n,n',q,\lambda} |M(n, n', q, \lambda)|^2 \, \Omega_{q,\lambda} \Pi_2(n', n, q_z, \Omega_{q,\lambda} + \omega_0) \times \left[n\left(\frac{\Omega_{q,\lambda}}{T}\right) - n\left(\frac{\Omega_{q,\lambda} + \omega_0}{T_e}\right) \right]. \tag{13}$$

Here $\omega_0 \equiv q_z v_d$, T denotes the lattice temperature, and $n(x) = (\exp(x) - 1)^{-1}$ is the Bose function. $\Pi_2(n', n, q_z, \omega)$ is the imaginary part of the electron–electron correlation function $\Pi(n', n, q_z, \omega)$. In the absence of dynamic screening, it takes the form

$$\Pi_0(n, n', q_z, \omega) = 2 \sum_{k_z} \frac{f(\varepsilon_n(k_z)) - f(\varepsilon_{n'}(k_z + q_z))}{\omega + \varepsilon_n(k_z) - \varepsilon_{n'}(k_z + q_z) + i\delta}.$$

The Fermi energy ε_F of this quasi-1D electron system (quantum wire) is determined from N_1 by the equation

$$N_1 = 2 \sum_{n,k_z} f(\varepsilon_n(k_z)).$$

Here $f(\varepsilon_n(k_z)) = \{\exp[(\varepsilon_n(k_z) - \varepsilon_F)/T_e] + 1\}^{-1}$ is the Fermi function.

The current through the quantum wire is $J = N_1 e v_d$ and the mobility is $\mu = v_d/E = -N_1 e v_d / F(v_d)$.

3. Numerical Results and Discussion

We have calculated the transport properties of quantum wires with radii ranging from 5 to over 30 nm and at lattice temperatures from 2 to 100 K in the absence of impurity scatterings. Fifteen subbands are included and form factors $F_{nn'}(q_\parallel)$ are obtained numerically.

Mobility and electron temperature are analyzed as functions of drift velocity. In carrying out the numerical calculation, we keep the electron volume density constant ($n_3 = 3.1831 \times 10^{17}$ cm^{-3}) for the bulk and all the quantum wire systems so that the electron wire density is given by $N_1 = n_3 \pi \varrho^2$. All the inter- and intrasubband scatterings due to bulk phonons (LA, TA, and LO) are taken into account, but the influence of surface phonons and confined phonons are ignored since they are expected negligible when the radius of the GaAs quantum wire is larger than 5 nm [5]. The matrix element of electron–phonon coupling and related parameters are the same as those given in [18].

Numerical calculation shows that the maximum of the intrasubband form factor $F_{nn}(q_\parallel)$ is at $q_\parallel = 0$ with $F_{nn}(0) = 1$ and $F_{nn}(q_\parallel)$ decreases to one half at about $q_\parallel = 2/\varrho$, and almost vanishes for $q_\parallel$ over $5/\varrho$. Therefore, if the radius of the quantum wire is very large, the intrasubband transition contributes to resistivity only when $q_\parallel \approx 0$. The intersubband form factors, on the other hand, increase from zero with increasing $q_\parallel (F_{nn' \neq n}(0) = 0)$ and arrive at their first maximum at $q_\parallel^m$ (1). Generally, several peaks exist (the position of the i-th peak is denoted by $q_\parallel^m(i)$). Thus the contribution of intersubband transitions comes mainly from large $q_\parallel$. These features of the form factors are illustrated in Fig. 1.

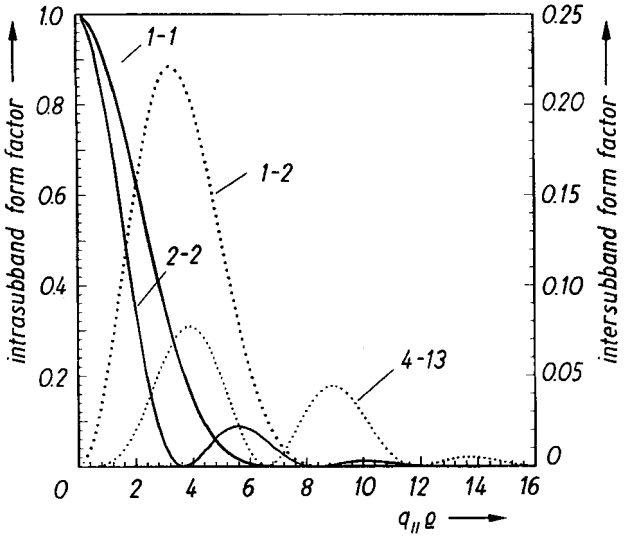

Fig. 1. Typical form factors of both intrasubband (solid curve) and intersubband (dotted curve) transitions as functions of normalized transverse wave vector $q_{\|}\varrho$

3.1 Crossover from 1D to 3D

The mobility of a quantum wire may be much higher or lower than that of the 3D system depending on the position of the Fermi energies relative to the subband bottoms. All fifteen subband energies measured from the ground subband are shown in Fig. 2a as a function of wire radius by thin dotted curves. The thick solid curve and thin solid curve in Fig. 2a denote, respectively, the linear mobility of the quantum wire and the corresponding Fermi energy at 2 K. When the radius of the wire is small, the mobility is very low because of the singularity of the one-dimensional density of states and the low Fermi energy. With the increase of the radius ϱ and corresponding rise of Fermi energy, the mobility increases rapidly until the Fermi energy touches the bottom of the second subband where the mobility reaches a maximum and then decreases steeply. The mobility exhibits a deep minimum following the sharp maximum, because the electrons can be scattered into the second subband easily when the Fermi energy is just below the second subband. Moreover, maximum and minimum show up repeatedly once the Fermi energy touches a new subband, exhibiting oscillations with the increase of quantum wire transverse size. The third peak in Fig. 2a is somewhat smaller because the corresponding subband is not degenerate.

Fig. 2b shows the linear mobility versus the wire radius at several lattice temperatures $T = 10$, 50 and 100 K (solid curves), and the corresponding 3D results are indicated by dotted lines. At higher temperatures, electrons with lower energy can also be scattered into the next subband, thus the peaks in the linear mobility move toward the smaller radius where the Fermi energy is lower. On the other hand, since the electron distribution function is broadened at higher temperatures, the amplitude of the mobility oscillation decreases and the curves approach the 3D cases.

High-field mobility and electron temperature as functions of wire radius are illustrated in Fig. 3 (solid curves mark mobilities, dotted ones represent the electron temperatures, and the horizontal bars denote the 3D cases). In Fig. 3a where $v_d = 7.935 \times 10^4$ m/s, $T = 10$ K, we can see that both the mobility and the electron temperature oscillate with

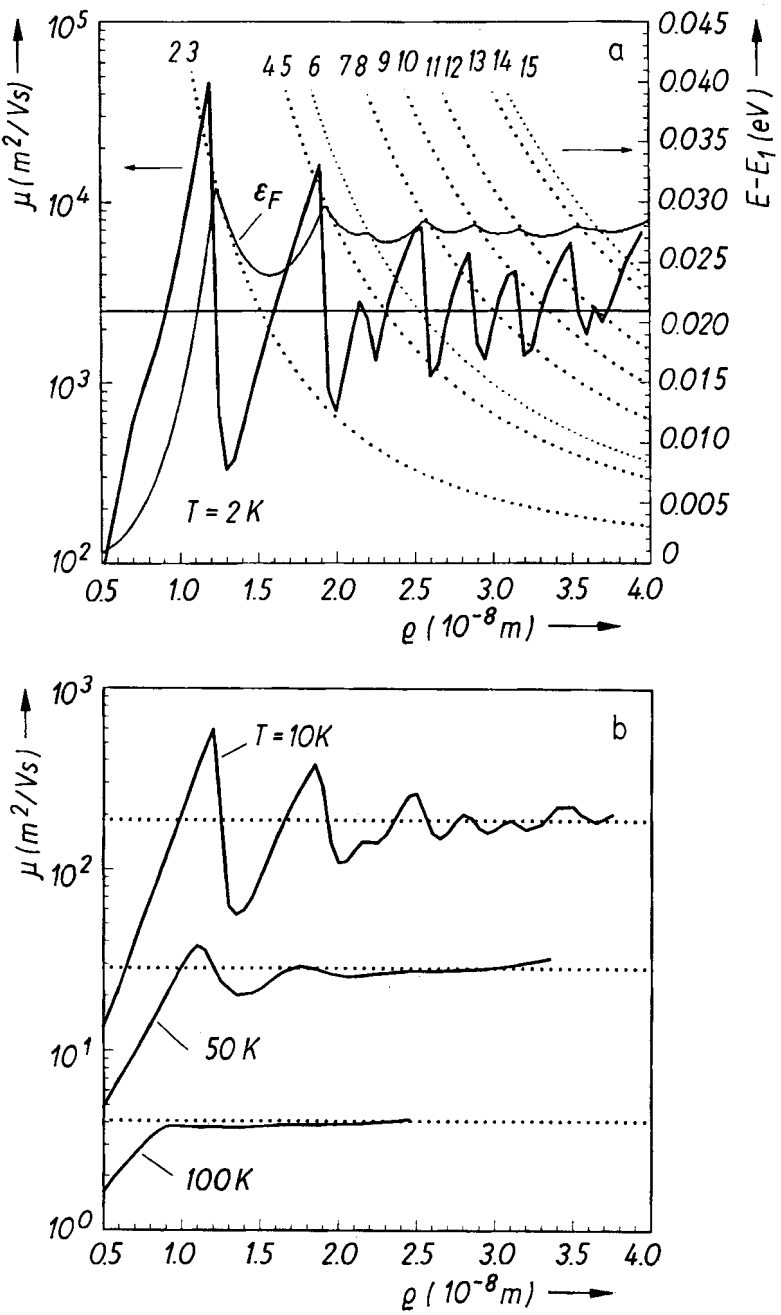

Fig. 2. a) Linear mobility μ (thick solid curve) and corresponding Fermi energy ε_F (thin solid curve) as functions of quantum wire radius ϱ and at lattice temperature $T = 2$ K. The long bar marks the mobility of the 3D case. The dotted curves represent associated subband energies (thick ones denote degenerate cases). Energies are measured from the ground subband, b) Linear mobility μ (solid curves) as function of quantum wire radius ϱ at different lattice temperatures (T = 10, 50, and 100 K). The dotted lines are results of the 3D system

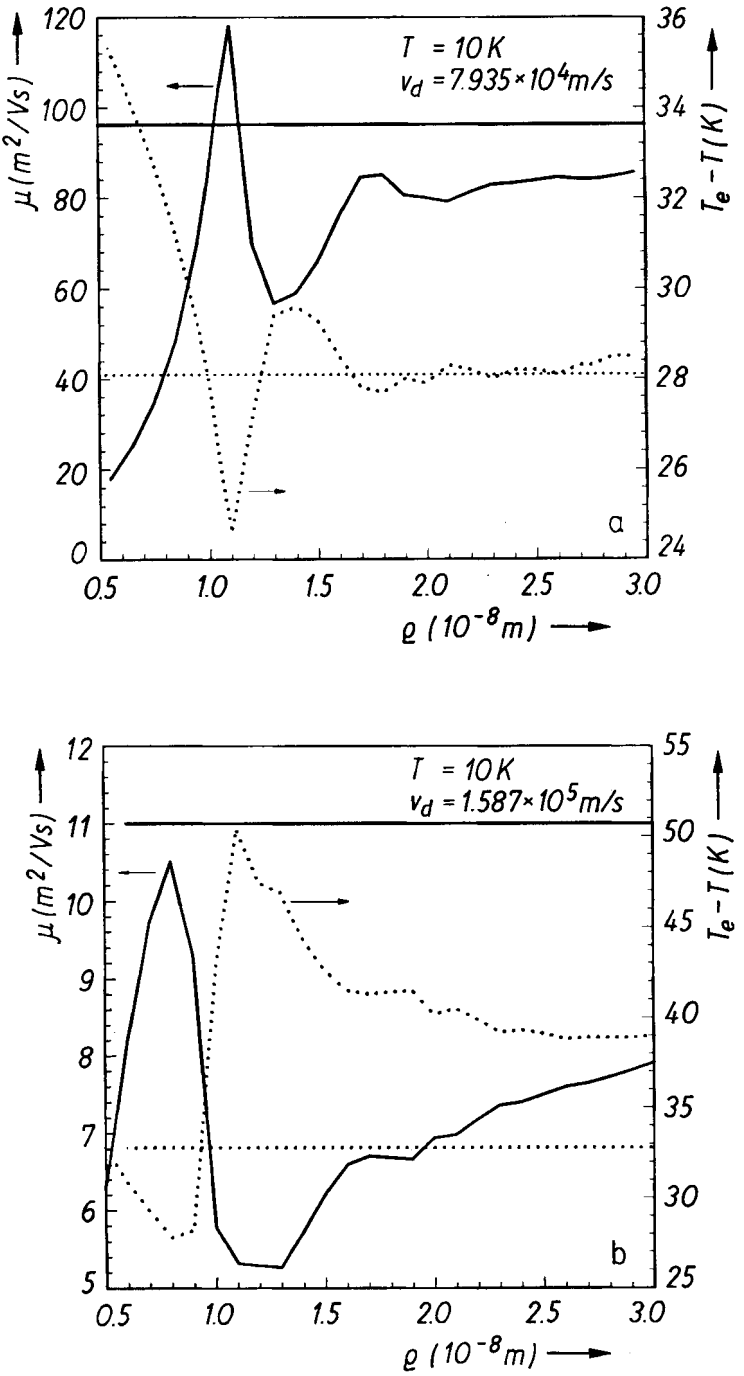

Fig. 3. High-field electron mobility μ (solid curve) and temperature difference $T_e - T$ (dotted curve) as functions of quantum wire radius ϱ at lattice temperature $T = 10$ K for a definite drift velocity a) $v_d = 7.935 \times 10^4$ and b) 1.587×10^5 m/s. The horizontal bars mark the corresponding 3D results

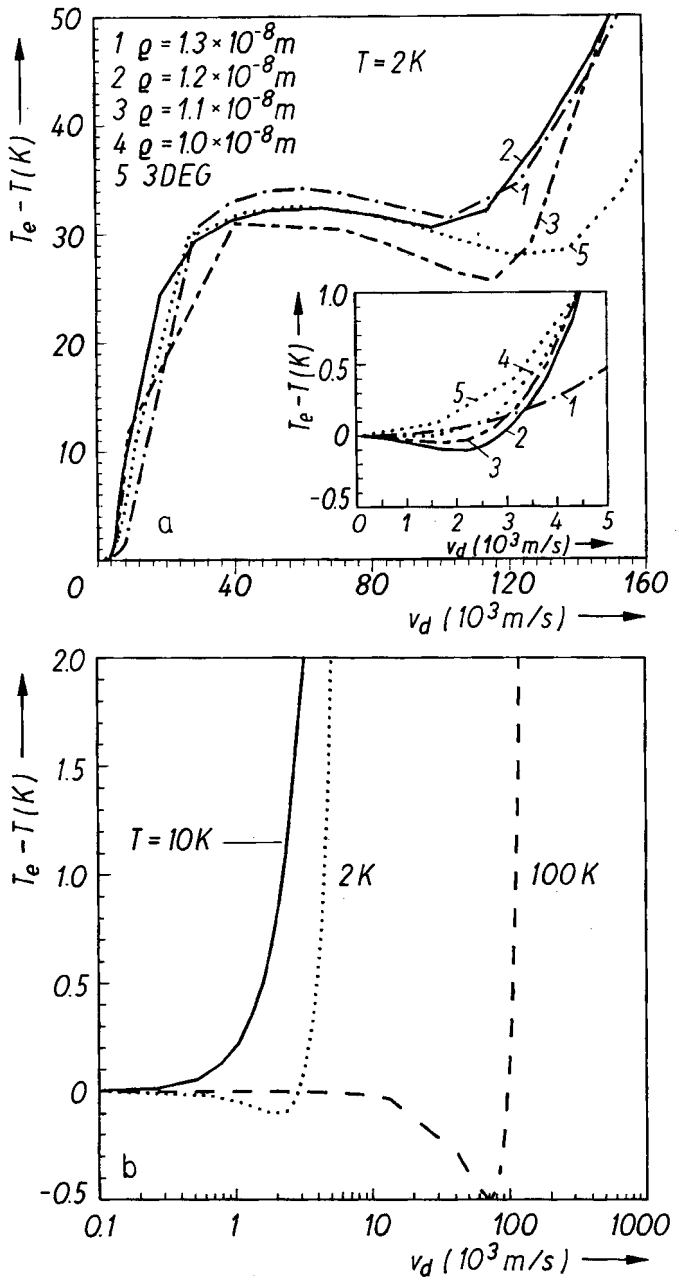

Fig. 4. a) The temperature difference $T_e - T$ as a function of drift velocity at lattice temperature $T = 2$ K for different quantum wire sizes. The result of the 3D system is marked by the dotted curve (5). The inset denotes the results of the low-field case, where cooling appears when the Fermi energy is at the top of subbands. b) Temperature difference $T_e - T$ as a function of drift velocity at different lattice temperatures. The radius of quantum wire $\varrho = 12$ nm. When lattice temperatures are low ($T = 2$ K) and high ($T = 100$ K), T_e may be lower than T. But T_e is always higher than T at medium temperature $T = 10$ K

increasing radius, but the mobility peaks correspond to the valleys of the electron temperature. This result is similar to that of [14]. The behavior of this mobility curve resembles the linear mobility one at lattice temperature $T = 50$ K because of the fact that the electron temperature $T_e \approx 40$ K, but the peaks move further to the small radius direction caused by the high drift velocity (the first one locates at $\varrho = 11$ nm). Another feature at high field is that the nonlinear mobility of the 1D system is lower than that of the 3D case. This is in contrast with the low-field case. In Fig. 3b, the drift velocity doubles and the electron temperature is $T_e \approx 50$ K. The first mobility peak is located at $\varrho = 8$ nm. As the wire radius ϱ is larger than 12 nm, the mobility (temperature) of electrons increases (decreases) with increasing ϱ. Both of them approach the results of the 3D case.

3.2 Cooling effect of the electrons

Just as in the 3D case, the electron temperature can be lower than the lattice temperature over a large range of drift velocities and reach a minimum at $v_d \sim v_{st}$ for very low lattice temperature when the piezoelectric interaction is the major scattering mechanism. When the Fermi energy is close to the top of the subband, the cooling effect becomes stronger as shown in Fig. 4a, where the Fermi energy reaches the top of the first subband for $\varrho = 12$ nm and comes into the bottom of the second subband at $\varrho = 13$ nm.

As the lattice temperature increases, the cooling disappears gradually until the contribution of the optical phonon plays an overwhelming role in momentum and energy relaxation. In Fig. 4b we plot the electron temperature as a function of v_d at different lattice temperatures ($T = 2$, $T = 10$, and $T = 100$ K) for a quantum wire of $\varrho = 12$ nm. At $T = 2$ K, the electron temperature may be 0.1 K lower than the lattice temperature when $v_d \approx v_{st}$. At $T = 10$ K, the electron temperature is never lower than the lattice temperature and no cooling can be observed at low electric field. As the lattice temperature rises to 100 K, because of the optical phonon contribution, the electron temperature is always lower than the lattice temperature until the drift velocity exceeds 9×10^4 m/s. The temperature difference $|T_e - T|$ is about 0.5 K at the minimum where v_d is about 7×10^4 m/s. It is worth noting that neglecting the influence of form factors will overestimate the temperature difference in the cooling effect.

The optical phonon-induced cooling can also be observed at low lattice temperature as shown up in Fig. 4a, where $(T_e - T)$ versus v_d curves at lattice temperature $T = 2$ K for different wire dimensions is represented. There are electron temperature minima in all curves around the drift velocity $v_d \approx 10^5$ m/s.

Those results are obtained without the influence of impurities. Generally, impurity-electron scattering will diminish or remove the cooling of electrons.

3.3 Nonlinear transport properties at high electric field

Fig. 5a depicts the nonlinear electron mobility μ versus v_d functions at lattice temperature $T = 2$ K with different wire radii ($\varrho = 11$ nm, $\varrho = 12$ nm, and $\varrho = 13$ nm) and they are compared with that of a 3D system (dotted curve). When the Fermi energy is on the top of the subband ($\varrho = 11$ nm and $\varrho = 12$ nm), the linear mobility of quantum wires is very high and the mobility decreases steeply with the increase of drift velocity because of the electron transition into the next subband. On the other hand, when the Fermi energy is at the bottom of the subband ($\varrho = 13$ nm), a mobility minimum appears at the drift velocity $v_d \approx 8 \times 10^3$ m/s, another multisubband effect.

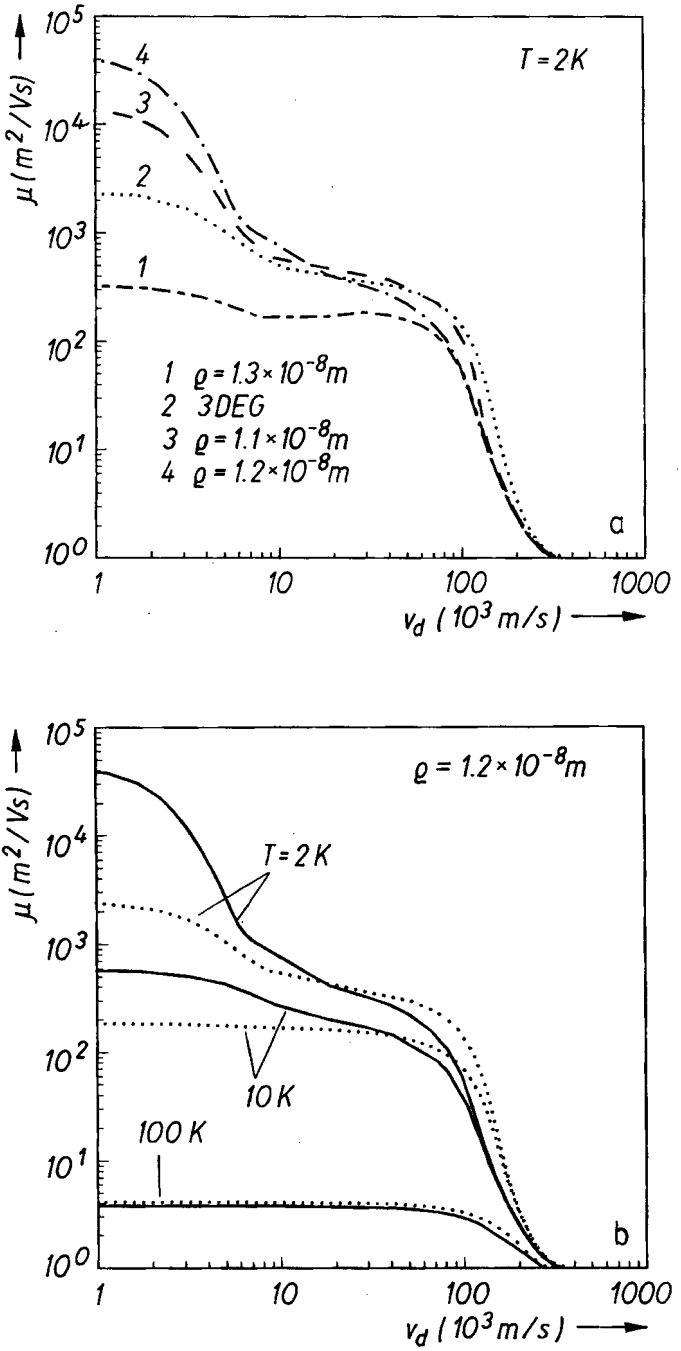

Fig. 5. a) Phonon-limited mobilities of the quantum wire as function of drift velocity (v_d) for different quantum wire radii at lattice temperature $T = 2$ K. b) Drift velocity (v_d) dependence of phonon-limited mobility (μ) of the quantum wire (solid curves) compared with that of a 3D system (dotted curves) at several lattice temperatures ($T = 2$, 10, and 100 K) for a definite quantum wire radius ($\varrho = 12$ nm)

In Fig. 5b, we calculate the mobilities of a quantum wire for a fixed radius (ϱ = 12 nm, solid line) and a 3D system (dotted curves) at different lattice temperatures (T = 2, 10, and 100 K). We find that at high temperature, the mobility of the quantum wire approaches to that of the 3D system.

It is worthy noting that the mobility plateau appearing in the drift velocity range $v_d \approx (10^4$ to $5 \times 10^4)$ m/s in Fig. 5 and the corresponding electron temperature saturation in Fig. 4a result from the saturation of the acoustic phonon scattering rate. In addition, we can find that mobilities in quantum wires are lower than those in the 3D system as shown in Fig. 5 and the electron temperature in quantum wires is relatively higher as depicted in Fig. 4 in the drift velocity regime $v_d \approx 1.5 \times 10^5$ m/s. This fact is a consequence of the displacement of mobility peaks (valleys) as the electric field increases as illustrated in Fig. 3. At extremely high electric velocity ($v_d > 3 \times 10^5$ m/s), the subband effcts are smoothed out by the high electron temperature and high drift velocity, such that the difference of mobility between quantum wires and 3D system disappears.

In conclusion, we have discussed both low-field and high-field transport properties of quantum wires with differing transverse radii as well as those of 3D systems. The electron mobility in quantum wires oscillates around that in a 3D system with increasing radius. At high lattice temperatures or extremely high fields, the mobility oscillation is suppressed and the conductance behavior is similar to those of 3D systems. Our results are qualitatively similar to those of experiments carried out by Ismail et al. [3].

References

[1] W. J. Skocpol, L. D. Jackel, E. L. Hu, R. E. Hu, R. E. Howard, and L. A. Fetter, Phys. Rev. Letters **49**, 952 (1982).

[2] P. M. Petroff, A. C. Gossard, R. A. Logan, and W. Wiegmann, Appl. Phys. Letters **41**, 635 (1982).

[3] K. Ismail, D. A. Antoniadis, and H. I. Smith, Appl. Phys. Letters **54**, 1130 (1989).

[3b] K. Ismail, W. Chu, R. T. Tiberio, A. Yen, H. J. Lezec, M. I. Shepard, C. R. Musil, J. Melngailis, D. A. Antoniadis, and H. J. Smith, J. Vacuum Sci. Technol. B **7**, 2025 (1989).

[4] H. Sakaki, Jr., J. appl. Phys. **19**, L735 (1980).

[5] J. P. Leburton and D. Jovanovic, Semicond. Sci. Technol. **7**, B202 (1992).

[6] M. R. Baldan, C. E. Leal, and I. C. da Cunla Lima, Phys. Rev. B **45**, 12091 (1992).

[7] K. W. Kim, M. A. Stroscio, A. Bhatt, R. Mickevicius, and V. V. Mitin, J. appl. Phys. **70**, 319 (1991).

[8] G. Fishman, Phys. Rev. B **34**, 2394 (1986).

[9] I. I. Boiko, Yu, M. Sirenko, and P. Vasilopoulos, Phys. Rev. B **43**, 7216 (1991).

[10] C. E. Leal, I. C. da Cunha Lima, E. A. de Andrada e Silva, and A. Troper, Phys. Rev. B **38**, 3225 (1988).

[11] T. Yamada and J. Sone, Phys. Rev. B **40** 6265 (1989).

[12] G. Y. Hu and R. F. O'Connell, Phys. Rev. B **43** 12341 (1991).

[13] U. Bockelmann and G. Bastard, Phys. Rev. B **42**, 8947 (1990).

[14] R. Mickevicius, V. V. Mitin, K. W. Kim, and M. A. Stroscio, Superlattices and Microstructures **11**, 277 (1992).

[15] R. Mickevicius, V. V. Mitin and K. W. Kim, J. Phys. Condensed Matter **4**, 4959 (1992).

[16] J. Lee and H. N. Spector, J. appl. Phys. **54**, 3921 (1983).

[17] X. L. Lei and C. S. Ting, Phys. Rev. B **30**, 4809 (1984); **32**, 1112 (1985).

[18] X. L. Lei, J. L. Birman, and C. S. Ting, J. appl. Phys. **58**, 2270 (1985); X. L. Lei and N. J. M. Horing, Internat. J. mod. Phys. B **6**, 805 (1992).

(Received September 3, 1992)